NJC

PAPER

Cite this: *New J. Chem.*, 2018, **42**, 9676

Fluorimetric and colorimetric analysis of total iron ions in blood or tap water using nitrogen-doped carbon dots with tunable fluorescence†

Fengjuan Liu, Yao Jiang, Chuan Fan, Liyan Zhang, Yue Hua, Chunxian Zhang, Ning Song, Yingjie Kong and Hua Wang *

Received 10th February 2018,
Accepted 5th April 2018

DOI: 10.1039/c8nj00711j

rsc.li/njc

Fluorimetric and colorimetric analysis strategies have been developed for simultaneously probing Fe^{3+} and Fe^{2+} ions in blood or tap water using nitrogen-doped carbon dots (N-Cdots). Herein, the N-Cdots were prepared using melamine by a neutralization heat reaction one-step synthesis route showing high aqueous solubility and environmental stability. Importantly, unlike common carbon dots (Cdots) that generally display one emission of blue fluorescence, they can display excitation-dependent tunable emissions. Moreover, the bright blue-green fluorescence of N-Cdots could be specifically quenched by Fe^{3+} or Fe^{2+} ions simultaneously, showing a color change. Herein, the fluorescent quenching of N-Cdots is thought to result from the aggregation of N-Cdots triggered by the unique coordination interactions between Fe^{3+} or Fe^{2+} ions and amine and amide groups of N-Cdots. The developed analysis strategies were employed for the evaluation of the total iron levels in blood or tap water, with a detection limit down to about 5.0 nM, exemplified for Fe^{3+} ions. These strategies could be promising for use in practical applications for the clinical diagnosis of iron-relative diseases (*i.e.*, anemia and cancers) and environmental monitoring of iron pollution. In addition, this one-step neutralization heat reaction route as a facile green synthesis candidate may be tailored for the fabrication of a variety of Cdots, especially those with doped heteroatoms (*i.e.*, nitrogen) for extensive applications in biomedical and environmental fields.

1. Introduction

Iron is an essential nutrient microelement that facilitates cell proliferation and growth and can play vital roles in human physiological and pathological activities.[1] Deficiency or excessive iron accumulation can induce some serious diseases, the most common of which is anemia.[2,3] Recent studies indicate that iron-dependent cell death, named ferroptosis,[4] can be induced in a subset of tumor cells, as iron encourages the formation of cancer-causing free radicals. An excessive amount of iron in the blood may indicate a high risk of cancer, thus serving as a potential target in the clinical diagnosis and therapeutics of various cancers.[5,6] However, iron possesses two kinds of valence state, Fe^{3+} and Fe^{2+}, which dynamically transform into each other, this makes it formidably difficult to detect Fe^{3+} or Fe^{2+} ions alone. Moreover, the total levels of Fe^{3+} and Fe^{2+} ions in environmental water, such as tap water, are a significant factor for the evaluation of water quality so as to prevent any iron-induced public health hazards.[7] Up to date, some quantitative strategies have been applied for the detection of iron, such as spectrophotometry,[8] atomic absorption spectrometry,[9] and mass spectrometry,[10] but they can involve complex bulk instrumentation and tedious sample preparation procedures.[11] Alternatively, many efforts have been devoted to the development of fluorimetric and colorimetric assays for the monitoring of iron using organic dyes[12–14] and metal nanoclusters.[15–17] Nevertheless, exploring a facile, efficient, and field-applicable detection method for probing total iron (Fe^{3+} and/or Fe^{2+} ions) is still of vital interest both for the diagnosis of iron-involved clinical diseases and for the environmental monitoring of water quality.

Recent years have seen the synthesis and increasing application of quantum dots (Qdots) for the detection of numerous targets of biomedical and environmental importance.[18–26] However, conventional metal semiconductor Qdots such as CdS, CdSe, and CdTe,[21,22,27–29] may have a risk of long-term biological toxicity and/or potential environmental hazards due to the use of heavy metal elements. Therefore, tremendous effort has been focused on the development of various Qdots that are

Institute of Medicine and Materials Applied Technologies, College of Chemistry and Chemical Engineering, Qufu Normal University, Qufu City, Shandong Province 273165, P. R. China. E-mail: huawangqfnu@126.com

† Electronic supplementary information (ESI) available: Synthesis conditions optimization, QY plotting, stabilization investigation, DLS analysis, XPS analysis, colorimetric ion tests, detection conditions optimization, colorimetric and fluorimetric sample analysis, and performance comparison among different detection methods. See DOI: 10.1039/c8nj00711j

environmentally friendly and biocompatible, most known as carbon dots (Cdots).[30–33] Compared to traditional metal semiconductor Qdots, Cdots can feature chemical inertness, aqueous solubility, and low toxicity. Up to date, a variety of synthesis methods have been developed for preparing Cdots, typically using the confined combustion and chemical oxidation routes,[34,35] which have the disadvantages of large time consumption, expensive precursors, operation difficulty, and low luminescent quantum yield (less than 10%).[36] However, it has been well established that Cdots doped with heteroatoms, for example, sulfur, nitrogen, and phosphorus elements, can achieve enhanced surface chemical activities, optical properties, and electronic characteristics.[22,33] As the most interesting example, nitrogen-doped Cdots (N-Cdots) can provide some distinct superior physicochemical properties such as high quantum yield, electrocatalytic activity, tunable luminescence, and biocompatibility,[37,38] promising potential applications in photocatalysis, photodetection, and bioanalysis or imaging.[39–44] For example, Zhang *et al.* reported the synthesis of N-Cdots by the hydrothermal route to serve as pH sensors for fluorescent environmental monitoring and bioimaging.[25] Tang *et al.* have synthesized nitrogen-doped Cdots with photoluminescence properties that are adjustable from blue to green emissions and can be applied in fluorescent inks and biocompatible staining.[45] In particular, it is widely recognized that N-Cdots can present better photoluminescence properties with an increasing percentage of nitrogen compared to the neighboring Cdots.[46] Nevertheless, the current methods for the fabrication of heteroatom-doped Cdots, especially those that are chemically nitrogen-doped, might encounter limitations such as a time-consuming synthesis, complicated purification, and environment-harmful surface modifications.[47]

In the present work, we report a facile and green synthesis strategy by a simple one-step neutralization heat reaction for the straightforward preparation of N-Cdots using the precursor melamine (MA), a nitrogen-rich organic molecule with three free amino groups and three aromatic nitrogen atoms, containing about 66.67% nitrogen. The resulting N-Cdots could display high aqueous solubility and environmental stability. Importantly, they could exhibit excitation-dependent tunable FL emissions, of which the blue-green fluorescence (FL) could be specifically quenched by both Fe^{3+} and Fe^{2+} ions simultaneously, showing an obvious color change. In contrast to most Cdots-based fluorimetric assays, that generally allow only for the detection of Fe^{3+} ions,[22,25,31,48,49] the developed fluorimetric and colorimetric strategies using N-Cdots could allow for the simultaneous analysis of Fe^{3+} and/or Fe^{2+} ions. Subsequently, the practical applications of the developed assays for total iron ions in blood or tap water were demonstrated, with the detection performances compared to those of other analysis methods for iron ions.

2. Experimental

2.1 Apparatus and reagents

Melamine (MA), ethylenediamine (EDA), and phosphoric acid were obtained from Aladdin Reagent Co. (Shanghai, China). De-ionized water was supplied from the ultrapure water system (Pall, USA). Other chemicals were of analytical grade and used directly without further purifications. All glass containers were cleaned using aqua regia and water before usage.

The FL measurements were conducted using a FL spectrophotometer (F-7000, Hitachi, Japan) operated at an excitation wavelength of 396 nm, with a slit width of 5.0 nm for both excitations and emissions. The signals of the FL intensities were collected at 470 nm. Transmission electron microscopy (TEM, FEI Tecnai G20, USA) imaging operated at 100 kV, and energy dispersive spectroscopy (EDS) were employed to characterize the N-Cdots and their iron-binding products. Moreover, UV-vis absorption spectra were recorded using a UV-3600 spectrophotometer (Shimadzu, Japan). Also, Fourier transform infrared (FTIR) spectra were obtained using a FTIR spectrophotometer (Thermo Nicolet Nexus 470 FT, USA). Furthermore, the hydrodynamic diameters of the N-Cdots were measured by dynamic light scattering (DLS) with a Zetasizer Nano ZS (Malvern Instruments, UK) setup equipped with a helium-neon laser (λ = 632.8 nm, 4.0 mW), of which the statistical analysis was conducted using the attached software. X-ray photoelectron spectra (XPS) were obtained using a Thermo ESCALAB 250Xi Multitechnique Surface Analysis (Thermo, USA). Additionally, the quantum yields (QY) of the as-prepared N-Cdots were measured by comparing the integrated intensities and absorbance values against the reference quinine sulfate, according to the measurement method reported elsewhere.[50] The QY of the yielded N-Cdots was thus calculated using the following equation:

$$Q_x = Q_{std}[I_x/A_x][A_{std}/I_{std}][\eta_x/\eta_{std}]^2$$

Here, the std and x represent the standard reference and the sample tested, respectively; Q and I separately refer to the measured quantum yield and integrated emission intensity; η and A are the refractive index and the optical density quantified *via* a UV-vis spectrophotometer, respectively.

2.2 Synthesis of fluorescent N-Cdots

N-Cdots were synthesized through the one-step neutralization heat reaction using MA as the precursor as illustrated in Scheme 1. Briefly, an aliquot of 60 mg MA was first added into 5 mL EDA to be dissolved ultrasonically. An aliquot of 3 mL phosphoric acid was poured into the solution quickly to be stirred vigorously for 2 min to yield the yellow products. After cooling down to room temperature, 25 mL ethanol was added into the mixture, followed by centrifugation at 12 000 rpm for 10 min to remove the salts. The supernatant was collected and subsequently purified by dialyzing against deionized water overnight using a dialysis membrane (pore size of 1.8 nm or molecular weight of 20 kD). Subsequently, the N-Cdot products were collected using the vacuum lyophilization method to be further stored in the dark at 4 °C for future usage.

2.3 Fluorimetric and colorimetric iron analysis

The fluorimetric and colorimetric detection methods were conducted separately for Fe^{3+} and/or Fe^{2+} ions, by simply mixing with an aliquot of N-Cdots re-dispersed in centrifuge tubes.

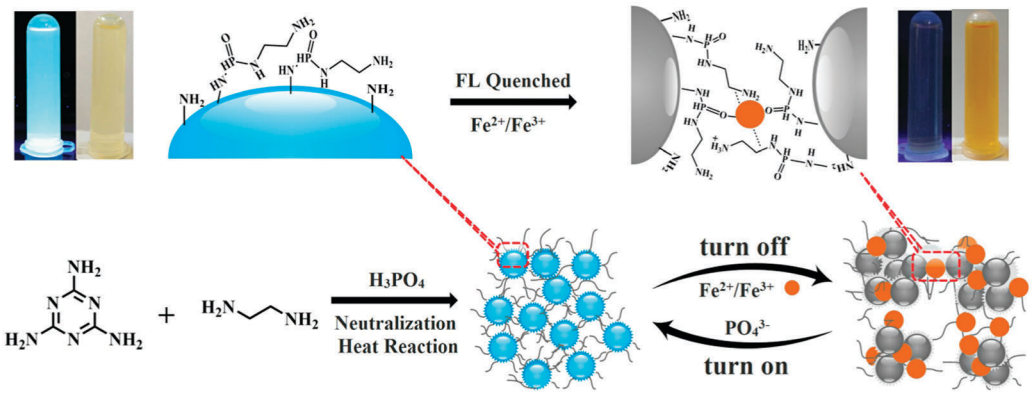

Scheme 1 Schematic illustration of the main mechanism of neutralization heat reaction for the fabrication of N-Cdots and the N-Cdots-based detection procedure for sensing Fe^{3+} or Fe^{2+} ions, where the FL of N-Cdots could be turned off once introducing Fe^{3+} or Fe^{2+} ions together with a color change, and would be turned on if PO_4^{3-} ions were added in high enough concentrations.

The FL intensities (λ_{ex} = 396 nm) of the N-Cdots were recorded, of which the FL quenching efficiencies of the probes were calculated according to the following equation: quenching efficiencies = $F_0 - F/F_0$, where F_0 and F refer to the FL intensities of N-Cdots in the absence and presence of testing ions, respectively. Moreover, the colorimetric analysis was performed for Fe^{3+} and/or Fe^{2+} ions and the UV-vis absorbances of the product solutions were recorded (λ_{max} = 475 nm). In addition, the fluorimetric and colorimetric responses to Fe^{3+} or Fe^{2+} ions (1.0 μM) were performed by comparing with other possibly co-existing interferential ions (10 μM) as the control tests included Ag^+, Hg^{2+}, Pb^{2+}, Cu^{2+}, Zn^{2+}, K^+, Na^+, Cr^{3+}, Ca^{2+}, Mg^{2+}, Ba^{2+}, Mn^{2+}, and Ni^{2+} ions. Subsequently, the N-Cdots-based fluorimetric and colorimetric methods were employed separately for the separate detection of Fe^{3+} and Fe^{2+} ions in buffer (0–10 μM) under the optimized conditions of 0.24 mg mL^{-1} N-Cdots, 124 mM NaCl, pH 8.0, and 37 °C.

In addition, the developed detection methods were applied accordingly for the analysis of real samples by probing Fe^{3+} and/or Fe^{2+} ions separately spiked in blood or tap water with different concentrations (0–10 μM).

2.4 Collection of human samples

All the experiments were performed in compliance with the Ethical Committee Approval of China, and approved by the ethics committee at the College of Chemistry and Chemical Engineering, Qufu Normal University. Additionally, human samples of blood were provided by the University Hospital at Qufu Normal University, which were collected from healthy volunteers with informed consent.

3. Results and discussion

3.1 Synthesis procedure and sensing principle of N-Cdots

It is well established that nitrogen doped in Cdots could create high defect levels of recombination centers to tune the charge transfer of Cdots with improved optical performances.[51] In the present work, nitrogen-doped N-Cdots were synthesized by a one-step neutralization heat reaction using MA as a nitrogen-rich organic molecule as the precursor. The main synthesis mechanism and the sensing procedure for the N-Cdots for probing Fe^{3+} and/or Fe^{2+} ions are schematically illustrated in Scheme 1. Herein, the neutralization heat released from the reaction of EDA and phosphoric acid triggers an intermolecular condensation, dehydration, and subsequent carbonization of MA to yield N-Cdots, displaying tunable excitation-dependent emissions of FL as demonstrated afterwards. More importantly, the FL of N-Cdots could be specifically turned off by Fe^{3+} or Fe^{2+} ions simultaneously, with a color change as described in Scheme 1, which can be visually seen in the photographs. Interestingly, the quenched FL of N-Cdots would be turned on if PO_4^{3-} was added with high enough concentrations such as 170 mM for chelating Fe^{3+}/Fe^{2+} ions. The phenomenon of the static FL quenching of N-Cdots induced by Fe^{3+}/Fe^{2+} ions is thought to result from the formation of coordination bonds between the Fe^{3+} or Fe^{2+} ions and the amine and/or amide groups of the MA-sourced N-Cdots.[50,52] Also, the –OH and P═O groups anchored on the N-Cdots, which might originate from the phosphoric acid used, could interact with Fe^{3+} or Fe^{2+} ions,[50,53,54] as clearly described in the top panel of Scheme 1. As a result, the aggregation of N-Cdots would occur leading to FL quenching and the color change. However, the detailed formation and iron-response mechanism of N-Cdots including the functional groups for biomedical labelling should be explored in the future.

3.2 Main synthesis conditions of N-Cdots

The main conditions for the one-step synthesis of N-Cdots by the neutralization heat reaction were optimized (Fig. S1, ESI†). Firstly, three types of bases of EDA, NaOH, and triethylamine were separately employed to examine the effect of bases on the FL properties of the yielded N-Cdots (Fig. S1A, ESI†). It was discovered that EDA is the optimal base to be selected to obtain the strongest FL intensities at λ_{em} = 470 nm. Furthermore, Fig. S1B (ESI†) shows that N-Cdots can be produced with the strongest FL intensities at 7.5 mg mL^{-1} MA. Moreover, it was noted that the FL intensities of the N-Cdots could be dependent on the dosages of EDA (Fig. S1C, ESI†) and phosphoric acid in volumes (Fig. S1D, ESI†). Accordingly, an aliquot of EDA and

phosphoric acid at the volume ratio of 5 : 3 was selected as the optimal for preparing N-Cdots in the heat-releasing experiment.

3.3 Characterization of N-Cdots for iron sensing

FTIR spectroscopy was first recorded for the prepared N-Cdots by comparing with MA (Fig. 1A). Accordingly, the broad intense peak at 3362 cm^{-1} is attributed to the C–OH stretching vibration. The peaks at 2974 cm^{-1} and 2900 cm^{-1} are related to the stretching vibration of C–H. The peaks at 1577 cm^{-1} and 1450 cm^{-1} are related to the bending vibrations of N–H and C–N (primary amine), respectively. The peaks at 1050 cm^{-1} and 926 cm^{-1} belong to the stretching vibrations of C–H and P=O, respectively. Moreover, N-Cdots were discovered to display tunable FL of excitation-dependent emission features (Fig. 1B). When excited from 340 to 480 nm, the emission peaks of N-Cdots first become stronger and then gradually decrease, showing a remarkable red shift of the emission wavelength. This excitation property of N-Cdots is thought to involve the unique surface energy trap structure or the band gap transitions of the conjugated p-domains,[50] although the detailed mechanism should be explored further. Also, Fig. 1B indicates that two UV-vis absorption peaks are observed to be locate at 237 and 272 nm for N-Cdots, typically corresponding to the p–p* transition of the aromatic sp^2 domains from the carbon core[55] and the n–p* transition, respectively, compared to the characteristic absorption peak of MA (237 nm). Furthermore, the QY of the N-Cdots was measured by using the reference of quinine sulfate (Fig. S2A, ESI†), showing a QY of about 12.8%. The environmental stability of N-Cdots was explored (Fig. S2B, ESI†). It was discovered that the N-Cdots could be stored in water for over six months, with no significant change in the FL intensities. In addition, the photostability of N-Cdots was studied by exposing them under a xenon lamp (Fig. S2C, ESI†), showing that their FL intensities could be basically maintained during a 30 s exposure. The evidences above indicate N-Cdots made from MA feature unique FL and UV-vis absorption properties and high environmental stability which is expected for the wide analysis applications.

The fluorimetric spectra were comparably investigated for N-Cdots in the absence and presence of Fe^{2+} ions or Fe^{3+} ions (Fig. 2A). One can note that the FL of N-Cdots could be dramatically quenched either by Fe^{2+} or Fe^{3+} ions, which can be recovered when PO_4^{3-} ions are introduced, as can be seen in

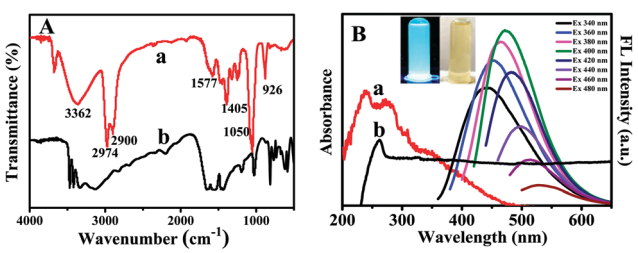

Fig. 1 (A) FTIR spectra of (a) N-Cdots and (b) MA. (B) UV-vis spectra (left) and FL spectra (right) of (a) N-Cdots and (b) MA, of which the FL emissions of N-Cdots are tunable at the different excitation wavelengths changing from 340 to 480 nm (inset: photographs of N-Cdots under UV light at 365 nm (left) and visible light (right)).

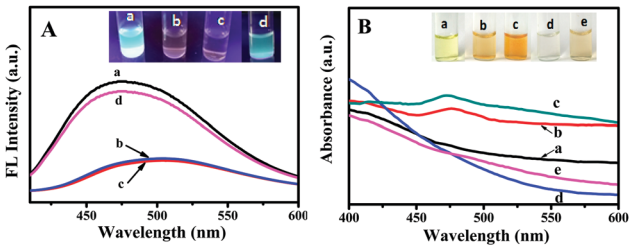

Fig. 2 (A) Comparison of fluorimetric spectra (λ_{ex} = 396 nm) of N-Cdots in the (a) absence and presence of (b) Fe^{2+} ions, (c) Fe^{3+} ions, and (d) Fe^{3+} or Fe^{2+} ions after adding PO_4^{3-} ions. (B) UV-vis spectra of N-Cdots in the (a) absence and presence of (b) Fe^{2+} ions and (c) Fe^{3+} ions, taking (d) Fe^{2+} ions and (e) Fe^{3+} ions solutions alone as the blank solutions for the comparison.

the corresponding photographs (inset). Herein, the coordination interactions between the N-Cdots and Fe^{3+} or Fe^{2+} ions might trigger their aggregation towards the FL quenching as aforementioned. Fig. 2B discloses the UV-vis spectra for the N-Cdots by comparison to those in the presence of Fe^{2+} or Fe^{3+} ions. Apparently, a color change of N-Cdots could occur simultaneously after adding Fe^{3+} or Fe^{2+} ions, as shown in the corresponding photographs (inset). Additionally, the FL of N-Cdots could be quenched once mixed with Fe^{3+} ions that were reduced by Fe powder (Fig. S3A, ESI†), thus confirming the Fe^{2+}-induced FL quenching of N-Cdots.

TEM imaging was conducted to investigate the topological structures of N-Cdots in the presence of Fe^{3+} ions as an example (Fig. 3). The morphology and size distribution results illustrate that the obtained N-Cdots have a uniform dispersity in water, clearly showing a quasi-spherical morphology of the N-Cdots (Fig. 3A). As shown in the magnified image (inset), the N-Cdots could display a lattice spacing of 0.24 nm, which might validate the sp^2 cluster structure of the N-Cdots. An average particle size of about 3.5 nm in diameter was determined by DLS analysis (Fig. S3B, ESI†). Furthermore, the addition of Fe^{3+} ions could induce the fluorescent probes to aggregate (Fig. 3B), which could

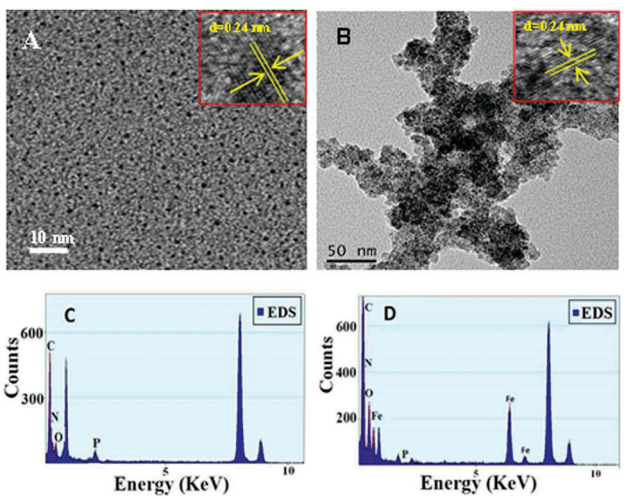

Fig. 3 TEM images of N-Cdots (A) before and (B) after adding Fe^{3+} ions (inset: the magnified images). EDS spectra of N-Cdots (C) before and (D) after adding Fe^{3+} ions.

be responsible for the FL quenching of N-Cdots. However, the aggregated particles of the N-Cdots retained their lattice spacing of 0.24 nm, showing an unchanged cluster structure. Moreover, the EDS analysis was conducted for N-Cdots (Fig. 3C). As expected, the N-Cdots could possess a composition of MA-sourced elements such as C and N atoms, showing the successful doping of nitrogen into the N-Cdots. Also, the O and P atoms could be included in N-Cdots, which could originate from the phosphoric acid used during the synthesis procedure. In addition, a comparable EDS analysis was performed for N-Cdots with Fe^{3+} ions, disclosing the additional presence of iron in the N-Cdots (Fig. 3D).

Furthermore, the chemical composition of the products of N-Cdots before and after adding iron ions were surveyed using the XPS spectrum, showing the typical signals of C, N, P and/or Fe elements and their bonding structures (Fig. S4, ESI†), these were consistent with those obtained by EDS analysis. In addition, the yielded N-Cdots could contain about 71.9% nitrogen according to the XPS measurements. These results confirmed that N and P atoms had been perfectly doped into the N-Cdots, which might aid improvement of the electronic and optical properties of N-Cdots, achieving the performance-improved fluorimetric analysis for iron ions.

3.4 N-Cdots-based fluorimetric and colorimetric iron analysis

The selective fluorimetric responses of N-Cdots to Fe^{3+} or Fe^{2+} ions were assessed in comparison to those of 15 other types of common metal ions that might possibly co-exist in the testing media (Fig. 4). As shown in Fig. 4A, only a little change to the FL intensities was observed for N-Cdots separately mixed with other competitive ions alone, even though they might have ten-time higher concentrations than the Fe^{3+} or Fe^{2+} ions. The obtained fluorescent responses are quantitatively shown in Fig. 4B, and can be clearly seen in the corresponding photographs (inset). More importantly, as can be seen from Fig. 4B, the fluorescent probes could present basically the same high responses to the Fe^{3+} or Fe^{2+} ions separately when co-existing with the other competitive ions tested. The data imply that the as-prepared N-Cdots could possess a considerably high selectivity in sensing Fe^{3+} and/or Fe^{2+} ions. Furthermore, Fig. S5 (ESI†) illustrates the colorimetric responses of N-Cdots to Fe^{3+} and/or Fe^{2+} ions in comparison to other ions indicated. It was discovered that N-Cdots could display the apparent color change when mixed with Fe^{3+} or Fe^{2+} ions, whereas no color change was obtained for N-Cdots mixed separately with the other ions indicated, as comparably manifested in their corresponding photographs of the reaction products (top). Therefore, the probes of N-Cdots could allow for the selective fluorimetric and colorimetric analysis of Fe^{3+} and/or Fe^{2+} ions.

3.5 Optimization of the analysis conditions

The main conditions of the N-Cdots-based analysis were explored using the fluorimetric detections of Fe^{3+} ions as an example (Fig. S6, ESI†). As can be seen from Fig. S6A (ESI†), the N-Cdots-Fe^{3+} interaction could be completed within 60 s. Moreover, the fluorimetric responses to the Fe^{3+} ions could depend on the ionic strengths of the NaCl concentrations, with the optimal one being 125 mM (Fig. S6B, ESI†). Also, the fluorimetric method could allow for the analysis of Fe^{3+} ions in the pH range from 5.0 to 10.0, with the maximized quenching efficiencies at pH 8.0 (Fig. S6C, ESI†). The temperature-dependent quenching efficiencies of N-Cdots revealed that 37 °C was the most suitable temperature to be chosen for the fluorimetric experiments (Fig. S6D, ESI†). These data indicate that the developed N-Cdots-based fluorimetric method could facilitate the rapid detection of Fe^{3+}/Fe^{2+} ions in widely applicable conditions.

3.6 Calibration curves for the iron analysis

Under the optimized conditions, the N-Cdots-based fluorimetric method was first employed for the separate detection of Fe^{3+} and Fe^{2+} ions in buffer (Fig. 5). It was observed that the FL intensities of N-Cdots could gradually decrease with the increasing concentrations of Fe^{3+} ions (Fig. 5A) or Fe^{2+} (Fig. 5B), with the photographs of

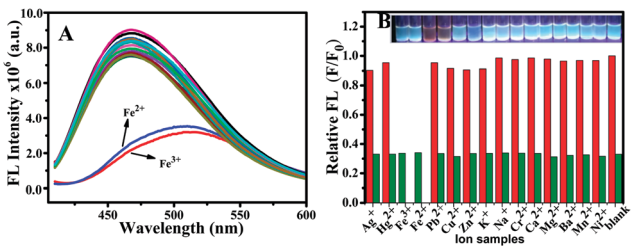

Fig. 4 (A) FL spectra (λ_{ex} = 396 nm) of N-Cdots separately with Fe^{2+} or Fe^{3+} (1.0 μM, pH 8.0) and other metal ions (10 μM) from top to bottom: blank, Ag^{+}, Hg^{2+}, Pb^{2+}, Cu^{2+}, Zn^{2+}, K^{+}, Na^{+}, Cr^{3+}, Ca^{2+}, Mg^{2+}, Ba^{2+}, Mn^{2+}, and Ni^{2+} ions, corresponding to (B) the changes of relative FL intensities of N-Cdots (0.24 mg mL^{-1}) (inset: the photographs of the product solutions under UV light), where the F_0 and F refer to the FL intensities of N-Cdots in the absence (red) and presence (green) of metal ions, respectively.

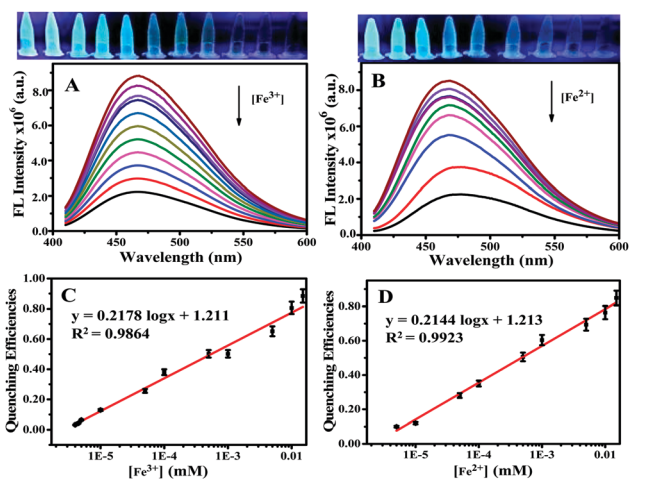

Fig. 5 FL spectra of N-Cdots separately with (A) Fe^{3+} ions and (B) Fe^{2+} ions of different concentrations (0–10 μM). The relationship between the FL quenching efficiencies of N-Cdots and different concentrations of (C) Fe^{3+} ions, and (D) Fe^{2+} ions in buffer (0–10 μM), with the photographs of corresponding testing solutions under UV light (top). The measurements were conducted in buffer under the optimized conditions of 0.24 mg mL^{-1} N-Cdots, 124 mM NaCl, pH 8.0, and 37 °C.

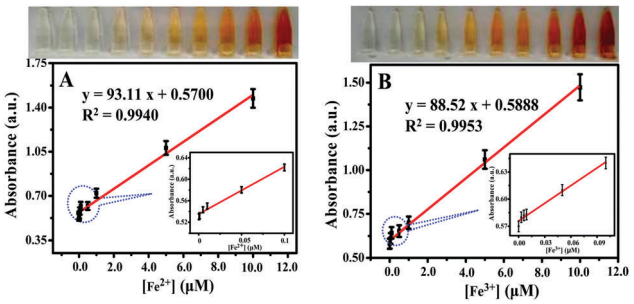

Fig. 6 Calibration detection curves of the N-Cdots-based colorimetric analysis describing the linear relationship of the absorbance values (λ_{max} = 475 nm) *versus* the different concentrations of (A) Fe^{3+} ions and (B) Fe^{2+} ions in buffer (0–12 μM), with the photographs of corresponding testing solutions under white light (top). The detections were performed under the optimized conditions of 0.24 mg mL^{-1} N-Cdots, 124 mM NaCl, pH 8.0, and 37 °C.

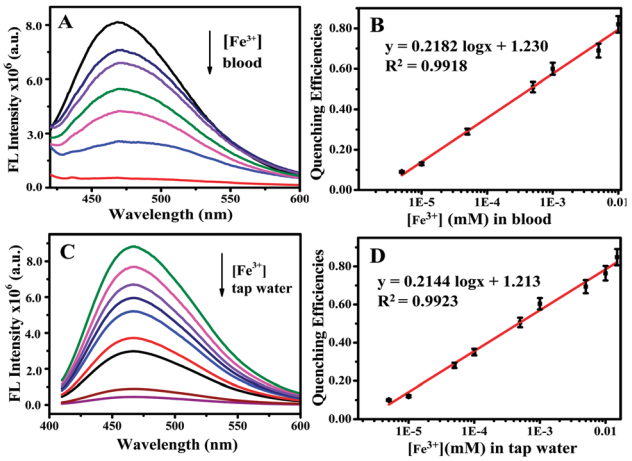

Fig. 7 Typical FL spectra (λ_{ex} = 396 nm) of the N-Cdots-based fluorimetric assays for Fe^{3+} ions of different levels separately spiked in (A) blood or (C) tap water samples, corresponding to (B and D) the calibration detection curves describing the linear relationship of the quenching efficiencies *versus* different concentrations of total Fe^{3+} ions, respectively. The sample analysis experiments were performed under the optimized conditions of 0.24 mg mL^{-1} N-Cdots, 124 mM NaCl, pH 8.0, and 37 °C.

the corresponding reaction products (top). Accordingly, the relationship between the quenching efficiencies and the logarithms of the Fe^{3+} concentrations was obtained in the linear ranges from 0.010 to 10.0 μM (R^2 = 0.9864), with a limit of detection (LOD) of about 5.0 nM, estimated by the 3σ rule (Fig. 5C). Also, Fe^{2+} ions could be detected in the linear concentration ranging from 0.020 to 10 μM (R^2 = 0.9923), with a LOD of about 7.5 nM (Fig. 5D).

Moreover, Fe^{3+} and Fe^{2+} ions were separately determined using the N-Cdots-based colorimetric method under optimized conditions using 0.24 mg mL^{-1} N-Cdots (Fig. 6). A colorimetric calibration curve was attained for describing the absorbance values *versus* the Fe^{3+} concentrations linearly ranging from 0.050 to 12.0 μM (R^2 = 0.9940), with a LOD of about 12.5 nM (Fig. 6A). Moreover, Fig. 6B shows that the detection calibration curve for the absorbance values of N-Cdots are linearly related to the different Fe^{2+} concentrations from 0.10 to 12 μM (R^2 = 0.9953). Therefore, the developed fluorimetric and colorimetric analysis methods with N-Cdots can allow for the simultaneous detection of Fe^{3+} and Fe^{2+} ions with a high detection sensitivity.

3.7 Applications for probing of Fe^{3+}/Fe^{2+} ions in samples

Under the optimized conditions, the fluorimetric analysis method with N-Cdots was first employed for Fe^{3+} ions spiked separately in blood or tap water with different concentrations (Fig. 7). One can observe from Fig. 7A that the FL intensities of N-Cdots could rationally decrease as Fe^{3+} concentrations increased. A calibration curve was thus obtained with the FL quenching efficiencies *versus* different concentrations of Fe^{3+} ions (Fig. 7B). Accordingly, Fe^{3+} ions in blood could be detected over the linear concentrations ranging from 0.050 to 10.0 μM (R^2 = 0.9918), with a LOD of 22.5 nM. Furthermore, the fluorimetric strategy was employed for the analysis of Fe^{3+}/Fe^{2+} ions in tap water, with the corresponding fluorescent spectra shown in Fig. 7C. A relationship between the quenching efficiencies and Fe^{3+} concentrations was attained, showing the linear Fe^{3+} concentrations ranging from 0.025 to 10.0 μM (R^2 = 0.9923), with a LOD of about 15 nM (Fig. 7D). Furthermore, to explore the feasibility of the practical applications, N-Cdots-based fluorimetric and colorimetric methods were employed to probe the total iron amounts of the Fe^{3+}/Fe^{2+} samples separately spiked in blood and tap water (Fig. S7, ESI†). Accordingly, total iron ions could be detected in basically the same ranges as they were when analyzed alone.

In addition, comparison of the detection performances was carried out for the developed N-Cdots-based fluorimetric method and other analysis methods using other types of probes for Fe^{3+} ions, and the data is summarized in Table S1 (ESI†). It was found that the developed fluorimetric strategy could display better or comparable analysis performances (*i.e.*, LOD) than other fluorimetric analysis methods reported elsewhere, thus promising possible application of the evaluation of iron levels in various practical samples.

4. Conclusions

In summary, nitrogen-doped N-Cdots were successfully synthesized by a one-step green synthesis route of the neutralization heat reaction. The yielded N-Cdots could present a strong blue-green FL, high aqueous solubility, and environmental stability. Importantly, they could display excitation-dependent tunable emissions that could be specifically quenched by Fe^{3+} or Fe^{2+} ions, simultaneously showing a color change. The N-Cdots were thereby employed for developing the fluorimetric and colorimetric assays for Fe^{3+} and/or Fe^{2+} ions, in contrast to common Cdots that generally display one emission of blue FL allowing for the detection of Fe^{3+} ions only. Moreover, the practical feasibility of the developed fluorimetric strategy was validated for simultaneously probing of Fe^{3+} and/or Fe^{2+} ions in blood or tap water samples with fairly high sensitivity and selectivity. The developed N-Cdots-based analysis method for total iron ions may have promise for potential application in the fields of

clinical diagnosis of iron-involved clinical diseases and environmental iron monitoring of water quality. In addition, this one-step green synthesis approach by the neutralization heat reaction may be extended for preparing various Cdots for biological sensing, labelling, and imaging applications.

Conflicts of interest

There are no conflicts to declare.

Acknowledgements

This work is supported by the National Natural Science Foundations of China (No. 21675099 and 21375075), the "Spark Program" of the Ministry of Science and Technology (No. 2015GA105005), and the Taishan Scholar Foundation of Shandong Province, P. R. China.

References

1 S. V. Torti and F. M. Torti, *Nat. Rev. Cancer*, 2013, **13**, 342–355.
2 N. Modepalli, S. Jo, M. A. Repka and S. N. Murthy, *Pharm. Res.*, 2013, **30**, 889–898.
3 S. Margetic, E. Topic, D. F. Ruzic and M. Kvaternik, *Clin. Chem. Lab. Med.*, 2005, **43**, 326–331.
4 S. Dixon, K. Lemberg, M. Lamprecht, R. Skouta, E. Zaitsev, C. Gleason, D. Patel, A. Bauer, A. Cantley and W. S. Yang, *Cell*, 2012, **149**, 1060–1072.
5 S. Fulda and D. Vucic, *Nat. Rev. Drug Discovery*, 2012, **11**, 109–124.
6 D. Ofengeim and J. Yuan, *Nat. Rev. Mol. Cell Biol.*, 2013, **14**, 727–736.
7 Q. Wang and C. Tan, *Anal. Chim. Acta*, 2011, **708**, 111–115.
8 S. Lunvongsa, M. Oshima and S. Motomizu, *Talanta*, 2006, **68**, 969–973.
9 J. E. Andersen, *Analyst*, 2005, **130**, 385–390.
10 A. Matusch, C. Depboylu, C. Palm, B. Wu, G. U. Höglinger, M. K. Schäfer and J. S. Becker, *J. Am. Soc. Mass Spectrom.*, 2010, **21**, 161–171.
11 S. Li, Y. Li, J. Cao, J. Zhu, L. Fan and X. Li, *Anal. Chem.*, 2014, **86**, 10201–10207.
12 J. C. Jin, L. Y. Pang, G. P. Yang, L. Hou and Y. Y. Wang, *Dalton Trans.*, 2015, **44**, 17222–17228.
13 X. Qu, Q. Liu, X. Ji, H. Chen, Z. Zhou and Z. Shen, *Chem. Commun.*, 2012, **48**, 4600–4602.
14 J. A. Ho, H. C. Chang and W. T. Su, *Anal. Chem.*, 2012, **84**, 3246–3253.
15 B. L. Hou, D. Tian, J. Liu, L. Z. Dong, S. L. Li, D. S. Li and Y. Q. Lan, *Inorg. Chem.*, 2016, **55**, 10580–10586.
16 C. X. Yang, H. B. Ren and X. P. Yan, *Anal. Chem.*, 2013, **85**, 7441–7446.
17 P. Wu, Y. Li and X. P. Yan, *Anal. Chem.*, 2009, **81**, 6252–6257.
18 S. Zhu, L. He, F. Zhang, M. Li, S. Jiao, Y. Li, M. Chen, X. E. Zhao and H. Wang, *Talanta*, 2016, **161**, 769–774.
19 T. T. Xu, J. X. Yang, J. M. Song, J. S. Chen, H. L. Niu, C.-J. Mao, S. Y. Zhang and Y. H. Shen, *Sens. Actuators, B*, 2017, **243**, 863–872.
20 S. W. Hu, S. Qiao, B. Y. Xu, X. Peng, J. J. Xu and H. Y. Chen, *Anal. Chem.*, 2017, **89**, 2131–2137.
21 H. Wang, J. Wang, C. Timchalk and Y. Lin, *Anal. Chem.*, 2008, **80**, 8477–8484.
22 B. Shi, Y. Su, L. L. Zhang, M. Huang, R. Liu and S. Zhao, *ACS Appl. Mater. Interfaces*, 2016, **8**, 10717–10725.
23 R. Liu, J. Zhao, Z. Huang, L. Zhang, M. Zou, B. Shi and S. Zhao, *Sens. Actuators, B*, 2017, **240**, 604–612.
24 M. Xue, L. Zhang, Z. Zhan, M. Zou, Y. Huang and S. Zhao, *Talanta*, 2016, **150**, 324–330.
25 B. Shi, Y. Su, L. Zhang, R. Liu, M. Huang and S. Zhao, *Biosens. Bioelectron.*, 2016, **82**, 233–239.
26 J. P. F. Angeli, M. Schneider, B. Proneth, Y. Y. Tyurina, V. A. Tyurin, V. J. Hammond, N. Herbach, M. Aichler, A. Walch and E. Eggenhofer, *Nat. Cell Biol.*, 2014, **16**, 1180–1191.
27 F. Shieh, A. E. Saunders and B. A. Korgel, *Cheminform*, 2005, **109**, 8538–8542.
28 Q. Ma, Y. Li, Z. H. Lin, G. Tang and X. G. Su, *Nanoscale*, 2013, **5**, 9726–9731.
29 Y. Yuan, J. Zhang, L. An, Q. Cao, Y. Deng and G. Liang, *Biomaterials*, 2014, **35**, 7881–7886.
30 B. Wang, Y. Chen, Y. Wu, B. Weng, Y. Liu and C. M. Li, *Microchim. Acta*, 2016, **183**, 2491–2500.
31 J. Yu, C. Xu, Z. Tian, Y. Lin and Z. Shi, *New J. Chem.*, 2016, **40**, 2083–2088.
32 B. Song, Y. Zhong, S. Wu, B. Chu, Y. Su and H. Yao, *J. Am. Chem. Soc.*, 2016, **138**, 4824–4831.
33 M. Xue, L. Zhang, M. Zou, C. Lan, Z. Zhan and S. Zhao, *Sens. Actuators, B*, 2015, **219**, 50–56.
34 L. Tian, D. Ghosh, W. Chen, S. Pradhan, X. Chang and S. Chen, *Chem. Mater.*, 2009, **21**, 2803–2809.
35 H. Li, Z. Kang, Y. Liu and S. T. Lee, *J. Mater. Chem.*, 2012, **22**, 24230–24253.
36 H. Li, X. He, Y. Liu, H. Huang, S. Lian, S. T. Lee and Z. Kang, *Carbon*, 2011, **49**, 605–609.
37 Y. Li, Y. Zhao, H. Cheng, Y. Hu, G. Shi, L. Dai and L. Qu, *J. Am. Chem. Soc.*, 2015, **134**, 15–18.
38 C. Hu, Y. Liu, Y. Yang, J. Cui, Z. Huang, Y. Wang, L. Yang, H. Wang, Y. Xiao and J. Rong, *J. Mater. Chem. B*, 2012, **1**, 39–42.
39 S. Dey, A. Govindaraj, K. Biswas and C. N. R. Rao, *Chem. Phys. Lett.*, 2014, **6**, 203–208.
40 W. Wang, Y. C. Lu, H. Huang, J. J. Feng, J. R. Chen and A. J. Wang, *Analyst*, 2014, **139**, 1692–1696.
41 L. Wang, L. Zhang, B. Lu, L. Han and S. Dong, *Electrochem. Commun.*, 2013, **34**, 68–72.
42 L. Wang, Y. Yin, A. Jain and H. S. Zhou, *Langmuir*, 2014, **30**, 14270–14275.
43 Z. Yang, M. Xu, Y. Liu, F. He, F. Gao, Y. Su, H. Wei and Y. Zhang, *Nanoscale*, 2014, **6**, 1890–1895.
44 J. Niu, H. Gao, L. Wang, S. Xin, G. Y. Zhang, Q. Wang, L. Guo, W. Liu, X. Gao and Y. Wang, *New J. Chem.*, 2014, **38**, 1522–1527.
45 X. Chen, Q. Jin, L. Wu, C. H. Tung and X. Tang, *Angew. Chem., Int. Ed.*, 2014, **53**, 12542–12547.
46 Y. Li, J. Zhang, Q. Wang, Y. Jin, D. Huang, Q. Cui and G. Zou, *J. Phys. Chem. B*, 2010, **114**, 9429–9434.

47 L. Tang, R. Ji, X. Li, K. Teng and S. Lau, *J. Mater. Chem. C*, 2013, **1**, 4908–4915.
48 C. Caltagirone, A. Bettoschi, S. Murgia, V. Lippolis, F. Isaia, A. Bencini, C. Giorgi, D. Berti, M. Mamusa and L. Conti, *RSC Adv.*, 2015, **5**, 37385–37391.
49 L. Tang, Y. Li, R. Nandhakumar and J. Qian, *Monatsh. Chem.*, 2010, **141**, 615–620.
50 Y. Liu, Y. Liu, S. J. Park, Y. Zhang, T. Kim, S. Chae, M. Park and H. Y. Kim, *J. Mater. Chem. A*, 2015, **3**, 17747–17754.
51 Z. Ma, H. Ming, H. Huang, Y. Liu and Z. Kang, *New J. Chem.*, 2012, **36**, 861–864.
52 J. Yu, N. Song, Y. K. Zhang, S. X. Zhong, A. J. Wang and J. Chen, *Sens. Actuators, B*, 2015, **214**, 29–35.
53 K. Qu, J. Wang, J. Ren and X. Qu, *Chemistry*, 2013, **19**, 7243–7249.
54 Q. Xu, P. Pu, J. Zhao, C. Dong, C. Gao, Y. Chen, J. Chen, Y. Liu and H. Zhou, *J. Mater. Chem. A*, 2015, **3**, 542–546.
55 X. M. Wei, Y. Xu, Y. H. Li, X. B. Yin and X. W. He, *RSC Adv.*, 2014, **4**, 44504–44508.